

# Response of 4H-SiC Detectors to Ionizing Particles

Robert Bernat <sup>1,\*</sup>, Ivana Capan <sup>1</sup>, Luka Bakrač <sup>1</sup>, Tomislav Brodar <sup>1</sup>, Takahiro Makino <sup>2</sup>, Takeshi Ohshima <sup>2</sup>, Željko Pastuović <sup>3</sup> and Adam Sarbutt <sup>3</sup>

<sup>1</sup> Ruđer Bošković Institute, Bijenička cesta 54, 10000 Zagreb, Croatia; capan@irb.hr (I.C.); luka.bakri@gmail.com (L.B.); tbrodar@irb.hr (T.B.)

<sup>2</sup> National Institutes for Quantum and Radiological Science and Technology, 1233 Watanuki, Takasaki 370-1292, Japan; makino.takahiro@qst.go.jp (T.M.); ohshima.takeshi@qst.go.jp (T.O.)

<sup>3</sup> Australian Nuclear Science and Technology Organisation, 1 New Illawarra Rd., Lucas Heights, NSW 2234, Australia; zkp@ansto.gov.au (Ž.P.); adam.sarbutt@gmail.com (A.S.)

\* Correspondence: rbernat@irb.hr

**Abstract:** We report the response of newly designed 4H-SiC Schottky barrier diode (SBD) detector prototype to alpha and gamma radiation. We studied detectors of three different active area sizes ( $1 \times 1$ ,  $2 \times 2$  and  $3 \times 3$  mm<sup>2</sup>), while all detectors had the same 4H-SiC epi-layer thickness of approximately  $\mu\text{m}$ , sufficient to stop alpha particles up to 6.8 MeV, which have been used in this study. The detector response to the various alpha emitters in the 3.27 MeV to 8.79 MeV energy range clearly demonstrates the excellent linear response to alpha emissions of the detectors with the increasing active area. The detector response in gamma radiation field of Co-60 and Cs-137 sources showed a linear response to air kerma and to different air kerma rates as well, up to 4.49 Gy/h. The detector response is not in saturation for the dose rates lower than 15.3 mGy/min and that its measuring range for gamma radiation with energies of 662 keV, 1.17 MeV and 1.33 MeV is from 0.5 mGy/h–917 mGy/h. No changes to electrical properties of pristine and tested 4H-SiC SBD detectors, supported by a negligible change in carbon vacancy defect density and no creation of other deep levels, demonstrates the radiation hardness of these 4H-SiC detectors.



**Citation:** Bernat, R.; Capan, I.; Bakrač, L.; Brodar, T.; Makino, T.; Ohshima, T.; Pastuović, Ž.; Sarbutt, A. Response of 4H-SiC Detectors to Ionizing Particles. *Crystals* **2021**, *11*, 10. <https://dx.doi.org/10.3390/cryst11010010>

Received: 4 December 2020

Accepted: 22 December 2020

Published: 24 December 2020

**Publisher's Note:** MDPI stays neutral with regard to jurisdictional claims in published maps and institutional affiliations.



**Copyright:** © 2020 by the authors. Licensee MDPI, Basel, Switzerland. This article is an open access article distributed under the terms and conditions of the Creative Commons Attribution (CC BY) license (<https://creativecommons.org/licenses/by/4.0/>).

**Keywords:** silicon carbide; radiation detector; radiation response; alpha particles; gamma radiation

## 1. Introduction

Silicon carbide, a wide band-gap semiconductor with exceptional thermal and mechanical stability [1,2], is now one of the most investigated materials for radiation particle detection. It has a very low leakage current, of an order of nA, which has a high influence in radiation detection applications [3]. The high threshold displacement energy of the material leads to a high level of radiation hardness compared with other common semiconductor detector materials [4,5], whereas the strong covalent bonds between atoms also makes the materials mechanically strong. Due to its radiation hardness, fast switching-capability, insensitivity to visible light, and biocompatibility, SiC is used for many other applications such as radiation hard electronics, high temperature coatings, biomedical sensors, UV-light sensors and others [6–9]. The radiation detectors based on 4H-polytype SiC epitaxial layers are mostly used as a charged particle [10,11] and neutron detectors [12]. In the past decades, the research on response of the 4H-SiC based detectors to charged particles and directly or indirectly, via neutron converters, to neutrons has been in focus. On the other hand, response of the 4H-SiC-based detectors to gamma radiation has not been extensively studied. Several authors reported on gamma and beta particle response of the SiC-based detectors, and were able to directly detect and distinguish different radiation types [10,13–15].

Our previously published results cover neutron detection testing activities performed at the Jožef Stefan Institute (JSI) TRIGA reactor in the framework of the E-SiCure project [12,16] with 4H-SiC SBD's with sizes of  $1 \text{ mm} \times 1 \text{ mm} \times 25 \mu\text{m}/69 \mu\text{m}$  and  $170 \mu\text{m}$  and using  $^6\text{LiF}$  and  $^{10}\text{B}_4\text{C}$  as converter films. In order to optimize neutron detection sensitivity of

4H-SiC detectors, it is necessary to understand the behavior of bare detectors in various radiation fields, other than the neutron one. Keeping in mind that the detection principle lie in the detection of charged particles, the response of the detector to alpha particles is of a particular importance. The best energy-resolution of 0.29% for 5486 keV alpha particles to date, has been reported by Mandal et al. [17] with 100% charge collection efficiency (CCE). The energy resolution was found to be dependent on the defect type and concentrations within the 4H-SiC epitaxial layers and on the noise of the detector and associated electronic modules of the detector system [11,17–19].

In this paper, we present comprehensive electrical characterization and radiation response of 4H-SiC detectors with different active surface areas (1 mm<sup>2</sup>, 4 mm<sup>2</sup> and 9 mm<sup>2</sup>) to different radiation fields. All 4H-SiC detectors have the same thickness of the epitaxial layers, which is 25 μm. We have used a wide range of alpha particles which covered energies up to 8.79 MeV, which was high enough to establish a connection between thickness of the epitaxial layer and particle energy. Testing the response of 4H-SiC detectors to gamma radiation was performed using Co-60 and Cs-137 calibration sources.

## 2. Materials and Methods

A typical SiC-based detector has the structure of an SBD, shown in Figure 1. Due to band alignment, a volume of depleted carriers is created at the semiconductor side of the junction, making the device very sensitive to the presence of electron-hole pairs generated upon illumination with above band-gap UV light or upon exposure to ionizing radiation. Since neutrons do not interact with valence electrons [20], their presence is deduced from the detection of ionizing neutron reaction products, like gamma rays, alpha particles, tritons, and larger ions. The SBD is operated under reverse bias, which increases the potential drop across the semiconductor and increases the depletion width. To limit the required operation voltage, the doping level of the substrate is usually two orders of magnitude higher than that of the epi-layer. Detailed specifications of 4H-SiC detectors have been reported elsewhere by several authors [18,21,22].

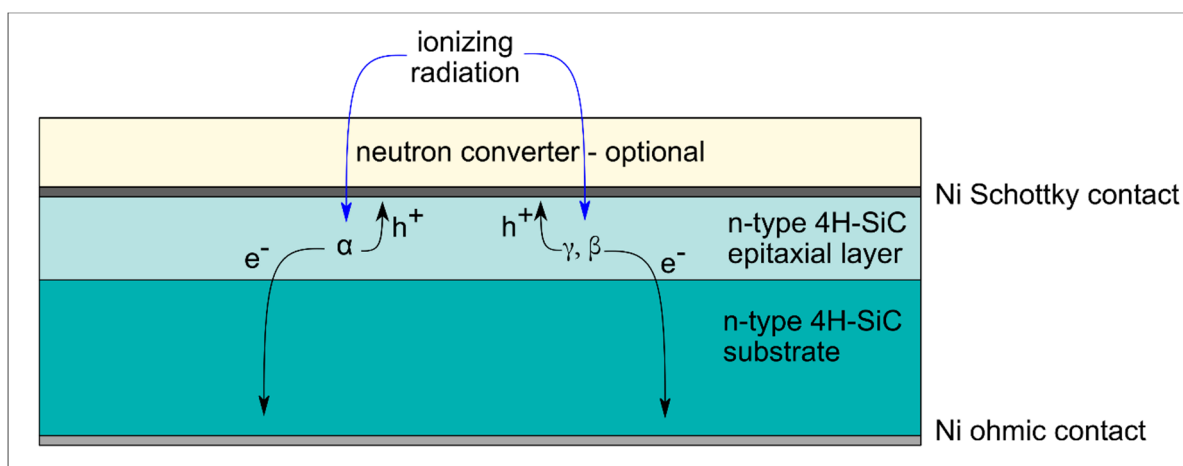


**Figure 1.** Design of a 4H-SiC SBD suitable for detection of ionizing radiation. A converter layer covering the front contact is optional and can substantially enhance the detection sensitivity to thermal neutrons.

4H-SiC SBDs were manufactured at the National Institutes for Quantum and Radiological Science and Technology in Japan (QST).

n-type SBDs were produced on nitrogen-doped (up to  $4.5 \times 10^{14} \text{ cm}^{-3}$ ) 4H-SiC epitaxial layers, approximately 25 μm thick [23]. The epitaxial layer was grown on the silicon face (8° off) of 350 μm-thick silicon carbide substrate without the buffer layer. The Schottky barrier was formed by thermal evaporation of nickel through a metal mask with patterned square apertures of  $1 \times 1 \text{ mm}^2$ ,  $2 \times 2 \text{ mm}^2$ , and  $3 \times 3 \text{ mm}^2$ , while Ohmic contacts

were formed on the backside of the silicon carbide substrate by nickel sintering at 950 °C in the Ar atmosphere.

The SBDs were mounted and wire-bonded onto chip carriers with two strip copper contacts. A coaxial cable (connected to the copper contacts on the chip carrier) was used to apply a reverse bias voltage to the SBD and to convey the signal to the data acquisition system. In order to isolate the detector components under high voltage, the chip carriers bearing the SiC SBDs were mounted into 3D printed plastic enclosures (Figure 2).

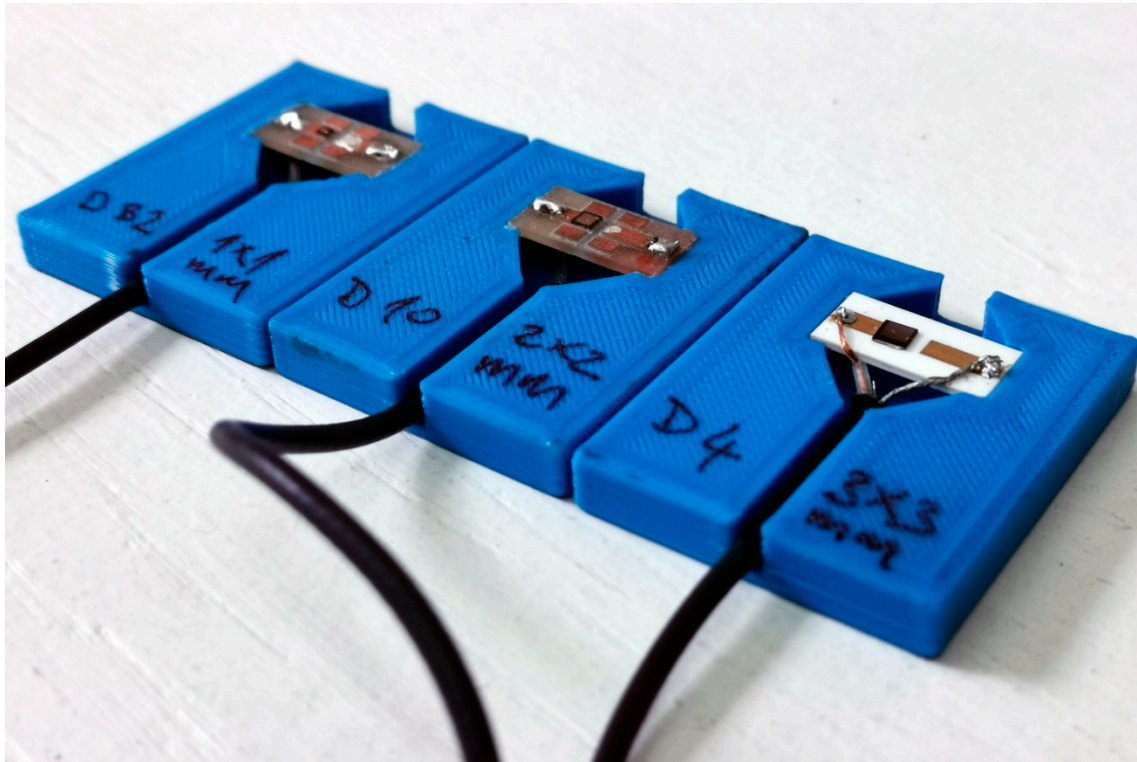


**Figure 2.** Three SBDs with different active volume were mounted into plastic enclosures.

The quality of the fabricated 4H-SiC SBDs was assessed by current-voltage (I-V) and capacitance-voltage (C-V) measurements. Measurements were carried out using a Keithley 6487 Picoammeter/Voltage Source and a Keithley 4200 Semiconductor characterization system (Keithley Instruments, Cleveland, OH, USA). Measurements were carried out in vacuum, at room temperature. Electrically active defects were characterized by deep level transient spectroscopy (DLTS) [24,25]. DLTS measurements were carried out in the temperature range from 150 to 400 K. The 4H-SiC detectors were cooled down from room temperature without an applied bias before DLTS measurements. The temperature ramp rate was 2 K/min. Capacitance transients were measured using a Boonton (Boonton Electronics, Parsippany, NJ, USA) 7200 capacitance meter using a 30 mV, 1 MHz sinusoidal signal.

We have made extensive studies of the 4H-SiC detectors response to the alpha particles, and we have used several alpha sources for testing and calibrations: mixed electroplated alpha source of Pu-239, Am-241 and Cm-244 ( $A = 3.7$  kBq), Th-228 alpha reference source ( $A = 3.7$  kBq), Gd-148 alpha particle standard ( $A = 3.7$  kBq), Pu-238 large area source (active area radius = 25 mm,  $A = 3.9$  kBq) and Am-241 large area source (active area radius = 25 mm,  $A = 3.4$  kBq). Due to its decay chain, Th-228 has seven energy maxima which are visible on the spectra. The reference date for all radionuclide activities is 06/24/2020. All measurements with alpha sources were performed in a vacuum chamber at 1 mbar.

Gamma irradiations were carried out at the Ruđer Bošković Institute's Secondary Standard Dosimetry Laboratory. We have used CIS Biointernational's radiotherapy calibration source of Co-60,  $A = 14.5$  TBq,  $K_a = 4.49$  Gy/h at source-to-surface distance (SSD) in a range from 1 m–5 m. We have also used Hopewell Designs' radiation protection standard sources of Co-60,  $A = 21.01$  GBq,  $K_a = 6.78$  mGy/h and Cs-137,  $A = 505.87$  GBq,  $K_a = 39.86$  mGy/h. The source of Cs-137 was used with additional attenuators with attenuating factors of 10, 100 and 1000. The air kerma rates at SSD = 1 m were 4.49 Gy/h, 383.11  $\mu$ Gy/h and 48.61  $\mu$ Gy/h respectively. Reference date for all gamma activities is 09/04/2020.

The electronic system used for measurements of signals induced in 4H-SiC SBDs consisted of a charge sensitive preamplifier (CREMAT CR-110, Cremat Inc, Newton, MA, USA), a Gaussian shaping amplifier (CREMAT CR-200-1 $\mu$ s), a multichannel analyzer (AMPTEK MCA 8000D, Amptek Inc, Bedford, MA, USA) and a laptop. Electrical power to the system was provided by a standalone battery-powered power supply in order to minimize the level of electronic noise. The reverse bias was applied to SBDs using a high voltage DC to DC converter (XP Power CA05P-5, XP Power, Singapore), also powered by the standalone power supply. The block diagram of the electronic system and its components is shown in Figure 3.

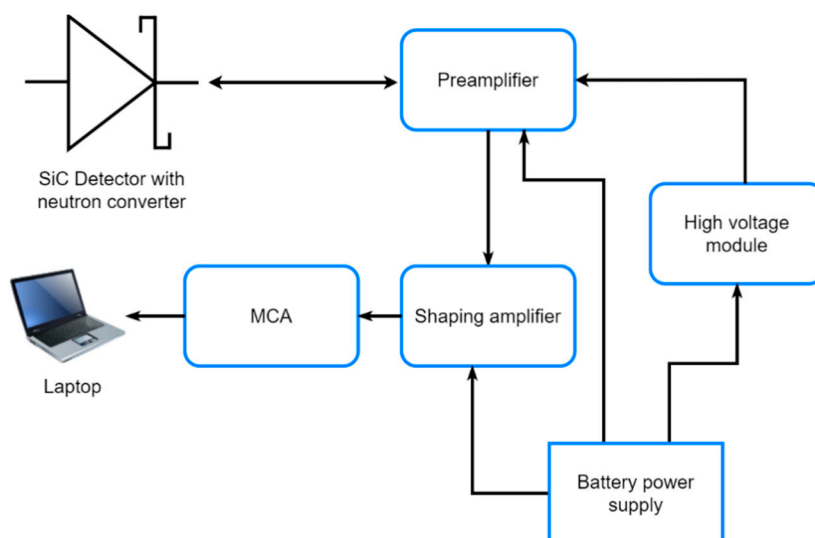


**Figure 3.** Block diagram of the detector system.

### 3. Results

The detector response was studied using alpha and gamma calibration sources. We have performed multiple irradiations of the detector prototype with various radiation sources in order to cover detection of a wide range of particle energy emissions. To observe both how irradiation affects the SBDs with a different active surface area, we performed thorough electrical characterization of SBDs before and after the irradiations.

#### 3.1. Electrical Characterization of SiC Detectors

The quality of the prepared SBDs has been checked by I–V and C–V measurements, before and after the irradiation tests. All selected SBDs showed excellent rectifying characteristics. For clarity, we show here I–V (Figure 4a) and C–V (Figure 4b) characteristics for only one SBD before and after radiation tests. It should be noted that radiation tests did not introduce any changes to electrical or rectifying properties of used SBD's. Measurements of electrical characteristics of all three 4H-SiC detectors are given in Supplementary files. The estimated 4H-SiC detector's parameters are given in Table 1.

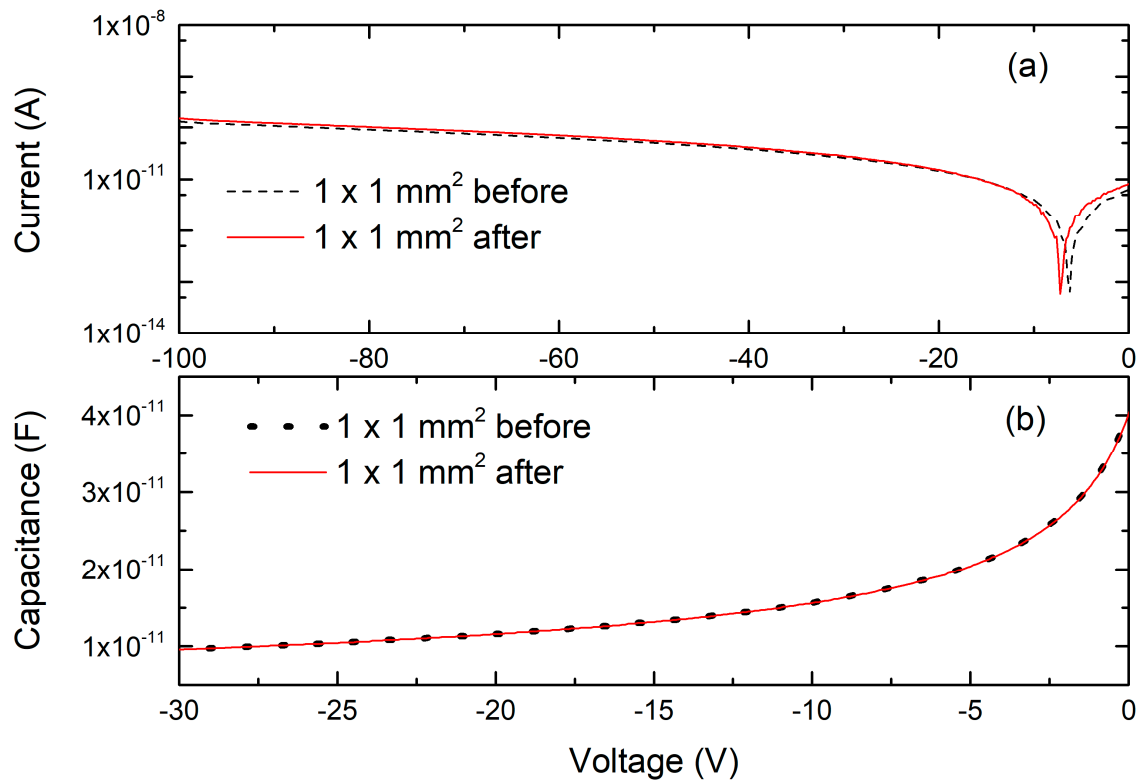


**Figure 4.** Measured electrical characteristics of 4H-SiC detector with active surface area of  $1 \times 1 \text{ mm}^2$  before and after radiation testing at room temperature: (a) I-V characteristics and (b) C-V characteristics.

**Table 1.** SBD parameters before and after radiation testing.

Sample		Ideality Factor	Schottky Barrier Height (eV)	Series Resistance ( $\Omega$ )	Free Carrier Concentration ( $\text{cm}^{-3}$ )
$1 \times 1 \text{ mm}^2$	Before	1.010	1.61	45	$4.4 \times 10^{14}$
	After	1.015	1.58	48	$4.4 \times 10^{14}$
$2 \times 2 \text{ mm}^2$	Before	1.003	1.64	35	$4.0 \times 10^{14}$
	After	1.080	1.55	65	$4.2 \times 10^{14}$
$3 \times 3 \text{ mm}^2$	Before	1.017	1.60	28	$4.7 \times 10^{14}$
	After	1.027	1.55	28	$4.7 \times 10^{14}$

Figure 5 shows DLTS spectra of the 4H-SiC detector (a) before and (b) after the irradiation test. One prominent deep level defect,  $Z_{1/2}$ , is observed in both the pristine 4H-SiC detector material and the irradiated detector material. The  $Z_{1/2}$  is a well-known deep level and previously assigned to a transition between double negative and neutral charge state of carbon vacancy  $V_C (= / 0)$  [26]. As recently reported [27,28], two emission lines,  $Z_1 (= / 0)$  and  $Z_2 (= / 0)$ , are resolved by the Laplace DLTS technique and assigned to carbon vacancies residing on two different lattice sites with local cubic and hexagonal symmetry. Carbon vacancy is acting as a strong recombination center and is thus the main life-time limiting defect in as-grown 4H-SiC, which is one of the crucial properties for radiation detectors and electronic devices in general [29]. Radiation tests did not introduce any new deep level defects or increased the concentration of a carbon vacancy, which is a good indicator of radiation hardness of tested 4H-SiC detectors. Determined activation energies and effective capture cross sections of electron emission for the observed deep level  $Z_{1/2}$  are given in Table 2.

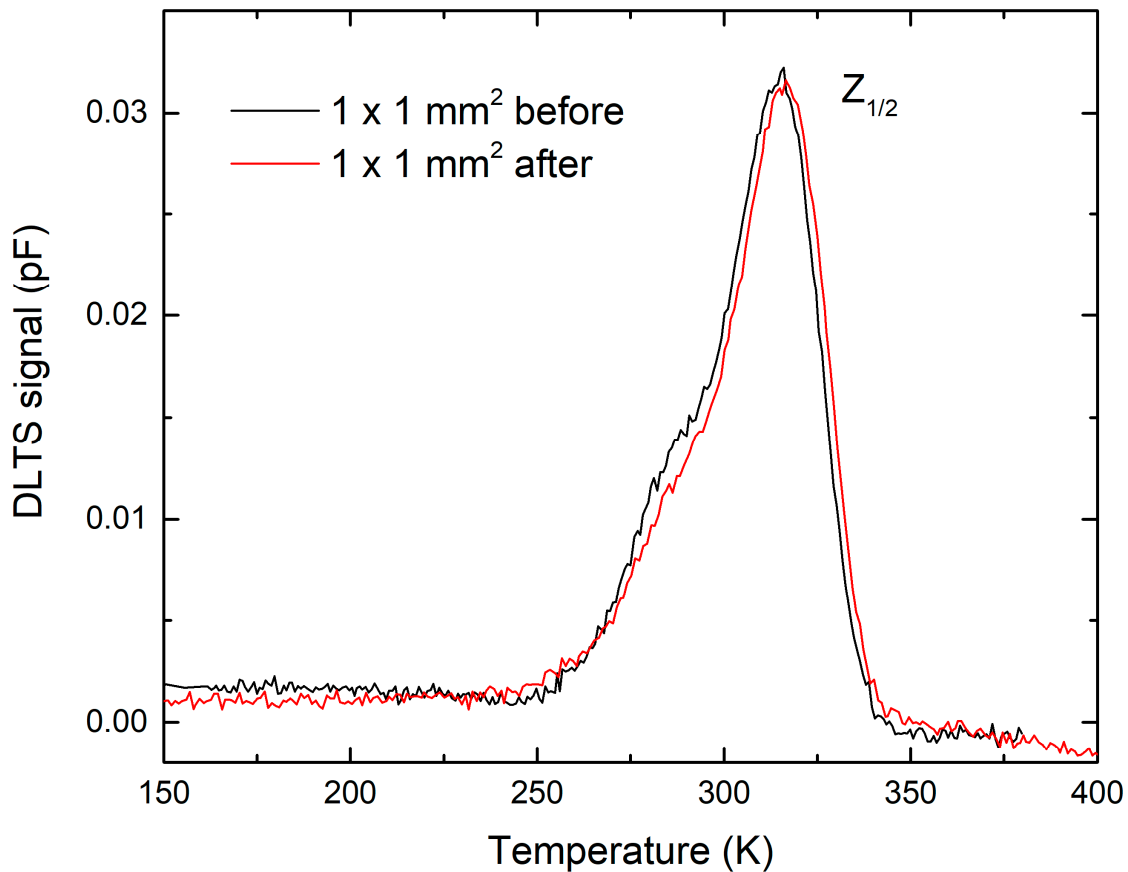


**Figure 5.** Shows a comparison of (a) DLTS spectra of the 4H-SiC detector with active surface area of  $1 \times 1 \text{ mm}^2$  before and after radiation tests. Measurements settings were: reverse voltage  $-10 \text{ V}$ , pulse bias  $-0.1 \text{ V}$ , pulse width  $10 \text{ ms}$ , and emission rate  $50 \text{ s}^{-1}$ .

**Table 2.**  $Z_{1/2}$  deep level parameters obtained from DLTS spectra of 4H-SiC detectors after radiation tests: activation energy,  $E_a$ , and effective carrier capture cross section,  $\sigma_a$ .

Sample	$E_a$ (eV)	$\sigma_a$ ( $\text{cm}^2$ )
$1 \times 1 \text{ mm}^2$	$0.68 \pm 0.01$	$9 \times 10^{-15}$
$2 \times 2 \text{ mm}^2$	$0.69 \pm 0.01$	$1 \times 10^{-14}$
$3 \times 3 \text{ mm}^2$	$0.67 \pm 0.01$	$6 \times 10^{-15}$

### 3.2. Response of 4H-SiC Detectors to Alpha Particles

All irradiations of 4H-SiC detectors with alpha particles having different energies were performed under low vacuum at 1 mbar, and a source—detector distance of 2 mm. Table 3 shows an overview of all radionuclides used in this study with its emission energies and yield per decay. The Am-241 isotope is the most common alpha emitter used for testing of particle detectors. It is also widely used for calibrating/checking gamma spectrometry systems. Apart from the Am-241, we have used a wide range of alpha emitters including those rarely used for radiation testing, like Gd-148 and Th-228.

**Table 3.** Overview of radionuclides used in this paper with their main emission energies and yield per decay [30].

Radionuclide	$\alpha$ Emission Energy/ies with Yield, (keV)	$\beta$ Emission Energy/ies with Yield, (keV)	$\gamma$ Emission Energy/ies with Yield, (keV)
Co-60	-	318 (100%), 1491 (<1%)	1173 (100%), 1333 (100%)
Cs-137	-	512 (95%), 1173 (5%)	662 (85%), 32 (6%)
Gd-148	3183 (100%)	-	-
Th-228 <sup>1</sup>	5340, 5423, 5685, 6050, 6288, 6778 and 8784	-	84 (1%)
Pu-238	5499 (71%), 5459 (29%)	-	16 (12%)
Pu-239	5156 (73%), 5143 (15%), 5105 (12%)	-	16 (6%)
Am-241	5486 (1%), 5443 (13%), 5388 (85%)	-	60 (36%), 18 (18%), 14 (13%)
Cm-244	5805 (76%), 5763 (24%)	-	17 (11%)

<sup>1</sup> Th-228 has many energy maxima due to its radioactive decay chain (Th-228—Ra-224—Rn-220—Po-216—Pb-212, Bi-212—Po-212—Pb—208).

Spectral response of detectors with an active area of  $2 \times 2 \text{ mm}^2$  to the mixed energy alpha particles is shown in Figure 6.

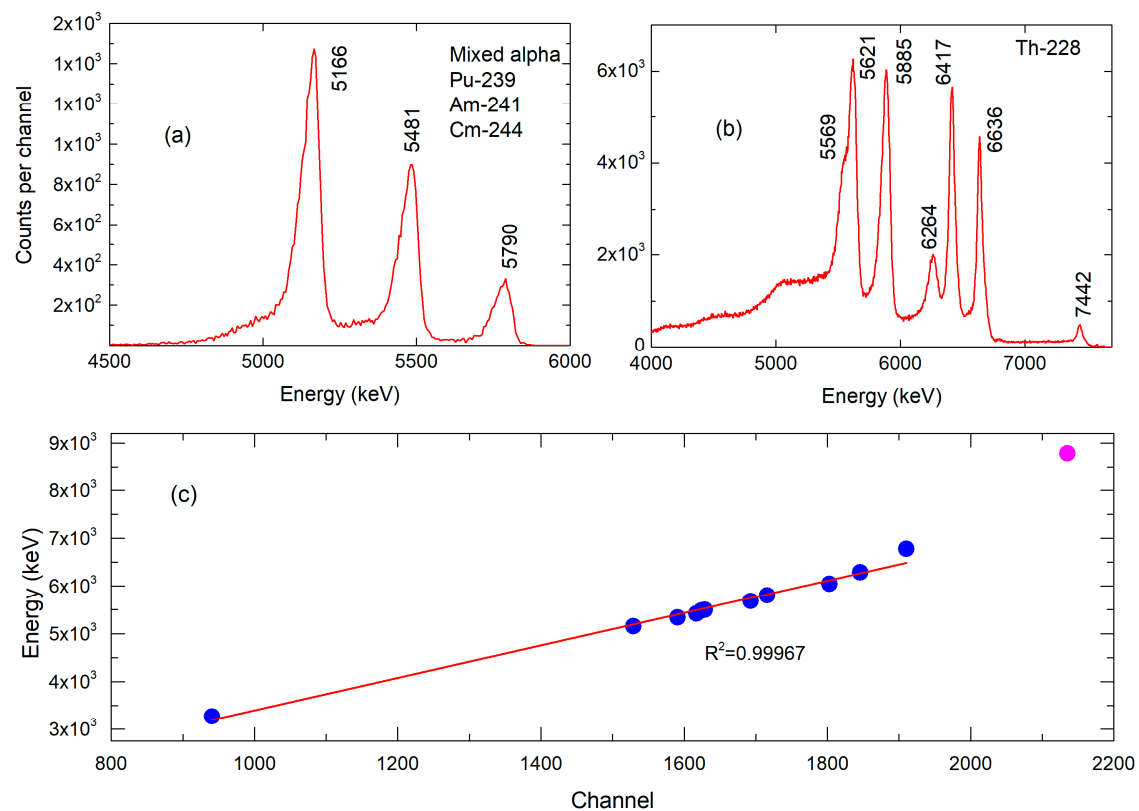


**Figure 6.** (a) Response of the 4H-SiC detector with active surface area of  $2 \times 2 \text{ mm}^2$  to mixed alpha particle source (Pu-239, Am-241, Cm-244) and (b) response of the same 4H-SiC detector to Th-228 alpha reference source. (c) Linear regression analysis of the 4H-SiC detector response over alpha decay energies of selected alpha particles, with active surface area of  $2 \times 2 \text{ mm}^2$ . The following alpha particle sources were used: Gd-148 ( $E_{\text{max}} = 3271 \text{ keV}$ ), Th-228 ( $E_{\text{max}}$  from its decay chain = 5340 keV, 5423 keV, 5685 keV, 6050 keV, 6288 keV, 6778 keV and 8784 keV), Pu-238 ( $E_{\text{max}} = 5499 \text{ keV}$ ), Pu-239 ( $E_{\text{max}} = 5157 \text{ keV}$ ), Am-241 ( $E_{\text{max}} = 5486 \text{ keV}$ ), and Cm-244 ( $E_{\text{max}} = 5805 \text{ keV}$ ). The 8784 keV energy is presented here to show nonlinear response of the 4H-SiC detector for the energies with a range in SiC higher than the epitaxial layer thickness.

The detector shows a linear energy response for the energies below 6.7 MeV with the R-Square value of 0.99967 as shown in Figure 6c. All specified energies of alpha particles are detected/observed. Furthermore, recorded peak intensity ratios reproduce tabulated values for the alpha particles with the end of particle range within the epitaxial layer thickness. The spectral response of our detector to Th-228 and its daughter products is better than the response obtained by Jarrell et al. [31], where different energy maxima in correlation with epitaxial layer thickness was used for the determination of the thickness of an electrodeposited thorium film.

In order to get additional information regarding the detector response to alpha particle irradiation, we have increased the active surface area of our detector. Figure 7 shows the response of the three detectors with  $1 \times 1 \text{ mm}^2$ ,  $2 \times 2 \text{ mm}^2$  and  $3 \times 3 \text{ mm}^2$  active area to the Am-241 alpha particle source. A large active area Am-241 source (diameter = 25 mm) was used to measure the response of 4H-SiC detectors with different active surface areas. A large area alpha source was used to minimize influence of the geometry to the response. Measurements were performed in vacuum for a time of 3600 s. Acquired spectra by all 4H-SiC detectors have characteristic Am-241 alpha decay peak at 5.486 MeV. Almost perfect linearity was established for alpha detection with different size detectors.

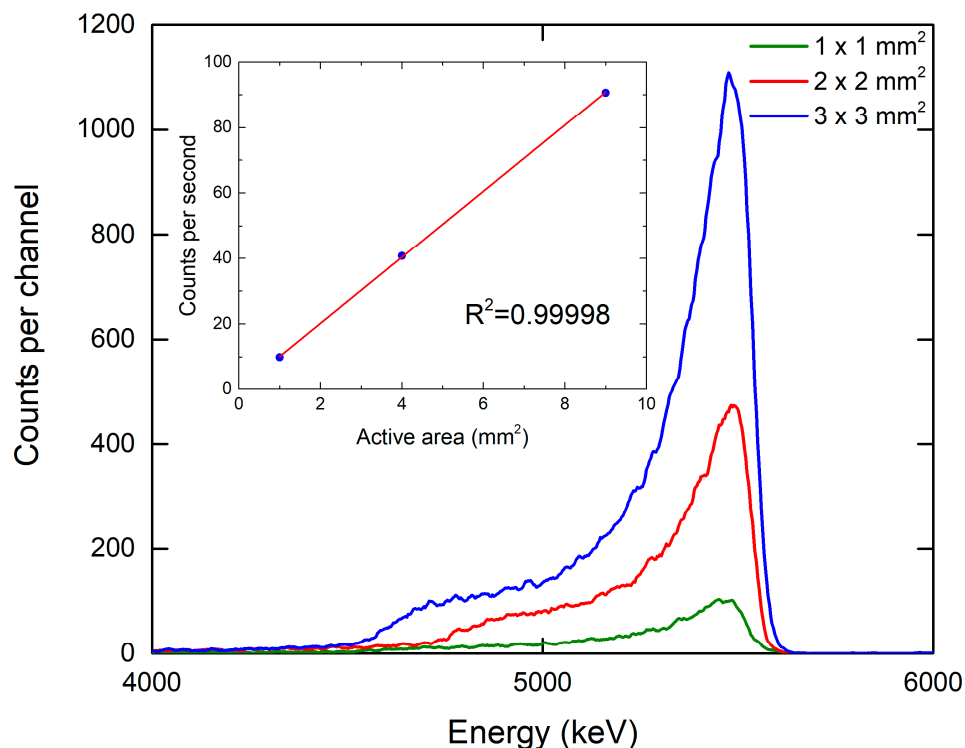


**Figure 7.** Response of 4H-SiC detectors with different active surface areas ( $1 \times 1 \text{ mm}^2$ ,  $2 \times 2 \text{ mm}^2$  and  $3 \times 3 \text{ mm}^2$ ) to the Am-241 alpha particles with linear regression. We can observe excellent collation of 4H-SiC detector response over the active detector area. There is no decrease in sensitivity of 4H-SiC detectors by increasing its active area.

It is expected that further enlargement of active detector areas, higher than  $3 \times 3 \text{ mm}^2$ , shall introduce a substantial amount of electronic noise and interferences.

All three detector sizes have an excellent spectral response for detection of various alpha emissions used in this work, except for the Po-212 alpha decay at 8785 keV (in Th-228 radioactive chain). We have covered energies from 3183 keV of Gd-148 to 6778 keV of Po-216 (in Th-228 radioactive chain), therefore we have linear response of our 4H-SiC detectors for the energies up to 6.8 MeV. The reason for the low efficiency of the 4H-SiC detector to 8785 keV alpha particles is the stopping power of the  $25 \text{ }\mu\text{m}$  SiC epitaxial layer. As simulated with SRIM (Stopping and Range of Ions in Matter [32,33]),  $37.7 \text{ }\mu\text{m}$  is the

range of 8.79 MeV alpha particles in SiC, and 24.6  $\mu\text{m}$  is the range of 6.7 MeV alpha particles in SiC.

Charge collection efficiency (CCE) of our fully depleted 4H-SiC detectors for detection of alpha particles from the large area Am-241 source is up to 100%. The best achieved energy resolution of our detector system, which was calculated from values of the full width at half maximum (FWHM), was 3% for the Am-241 energy of 5486 keV and 3.3% for Gd-148 energy of 3183 keV. The obtained energy resolution is similar to previously published results [11,17–19].

### 3.3. Response of 4H-SiC Detectors to Gamma Radiation

We have obtained broad signal distribution in the low energy end of the spectra corresponding to partial deposited photon energy for ionization but above the electronic noise cut-off for all gamma irradiations performed in air, under monitored environmental conditions ( $T = 18.3\text{--}19.4\text{ }^\circ\text{C}$ ,  $p = 992.1\text{--}1001.7\text{ hPa}$ ). The epitaxial layer of SiC (25  $\mu\text{m}$ ) is not able to stop high-energy photons, therefore a well-defined spectral peak with Gaussian shape cannot be recorded in the photon energy spectrum.

We have noticed that irradiations of the 4H-SiC detector with a higher air kerma rate results in fewer counts per air kerma than the irradiations of the 4H-SiC detector with low air kerma rate. Slopes of the curves, intercept was fixed at 0, were  $12,860\text{ mGy}^{-1}$  for Figure 8a,  $11,007\text{ mGy}^{-1}$  for Figure 8b and  $5004\text{ mGy}^{-1}$  for Figure 8c. Although the 4H-SiC detector shows a linear response to dose while exposed to a high dose rate, as shown in Figure 8c, it should be mentioned that the 4H-SiC detector is in saturation, which will be explained later. Linear response of the SiC detector to the air kerma was noticed before [14] but not the linear response to the dose rate as well. It is not possible to discriminate pulse-high signals from the 4H-SiC detectors according to the gamma source energy. Although, Co-60 and Cs-137 sources are used mainly for gamma irradiations, they are also beta emitters. However, all gamma irradiations were performed through a thick PMMA layer so that beta particles could not reach the 4H-SiC detector with the intensity that would have a significant impact on results. SiC could have potential to be used as a gamma radiation detector, but its low limit of detection would be quite high—above  $0.5\text{ mGy/h}$ .

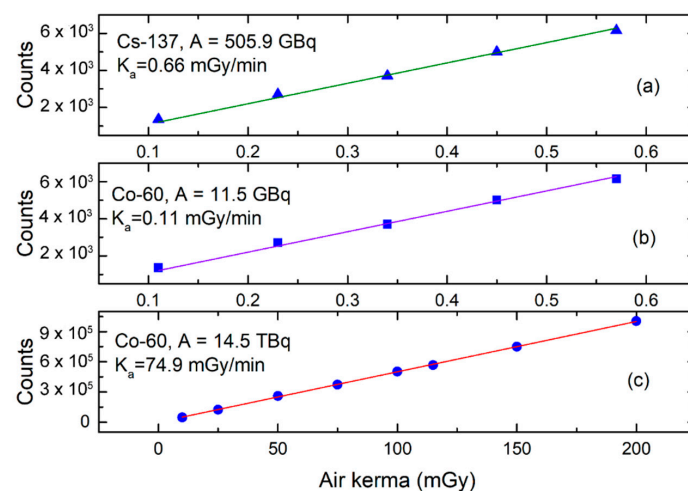


**Figure 8.** Response of 4H-SiC detector with active surface area of  $2 \times 2\text{ mm}^2$  to (a) Cs-137 source with activity of 505.9 GBq and to two Co-60 sources with activities of 14.5 TBq and 11.5 GBq, (b) and (c). Linear dose response of the 4H-SiC detector is observed for a stronger and weaker Co-60 source. However, different curve slopes suggest that the irradiations with lower air kerma rate results with creations of more electron-hole pairs per air kerma than the higher air kerma rate. The same behavior was observed for 4H-SiC detectors with  $1 \times 1\text{ mm}^2$  and  $3 \times 3\text{ mm}^2$  surface area, but for clarity, only measurements with  $2 \times 2\text{ mm}^2$  4H-SiC detector is presented here.

We have made multiple irradiations of the 4H-SiC detector with an active surface area of  $2 \times 2 \text{ mm}^2$  with the same air kerma while changing the air kerma rate, as shown in Figure 9. While exposed to dose rates of 15.29 mGy/min and lower, 4H-SiC detector leaves the so-called saturation mode and is showing a constant count rate, which defines the upper limit of detection. Our detector system is limited, with a minimum input rise time of a multichannel analyzer (Section 2), therefore it cannot effectively detect pulses shorter than 500 ns. The delivered air kerma for all irradiations shown in Figure 9 was 50 mGy. For the same dose, response of the 4H-SiC detector is not constant while in saturation. When the dose rate fell below 15.29 mGy/min (shaded in blue color in Figure 9), the 4H-SiC detector's response was not related to the dose rate and remained a constant response rate with  $\sigma = \pm 2.7\%$ .

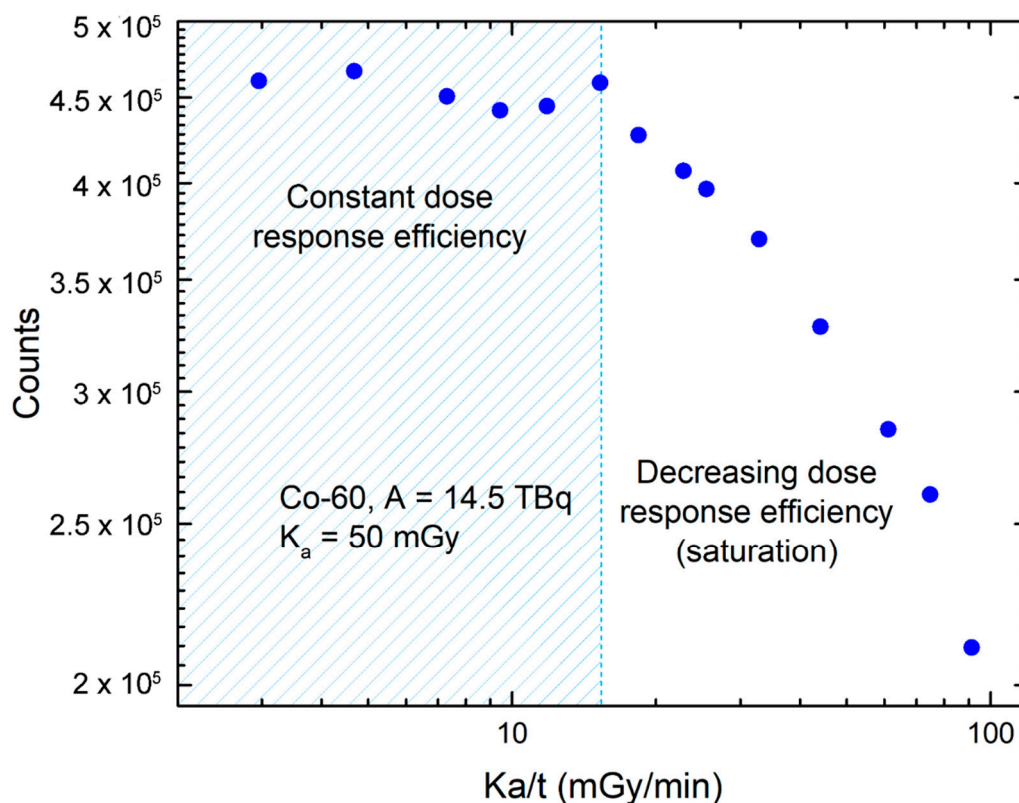


**Figure 9.** Response of 4H-SiC detector with active surface area of  $2 \times 2 \text{ mm}^2$  to Co-60 source with activity of 14.5 TBq. Irradiations with were performed with different air kerma rates.

We have tested the response of the 4H-SiC detector to a wide range of dose rates and the results show that the measuring range of 4H-SiC detector for gamma radiation with energies of 662 keV, 1.17 MeV and 1.33 MeV is from 0.5 mGy/h to 917 mGy/h.

Figure 10 shows the response of three different 4H-SiC detector sizes ( $1 \times 1 \text{ mm}^2$ ,  $2 \times 2 \text{ mm}^2$  and  $3 \times 3 \text{ mm}^2$ ) to gamma radiation. We can see that the gamma response over the size of the 4H-SiC detector is good. However, the sensitivity of the 4H-SiC detector with the largest active area is decreasing, which was not the case for the response of the SBD to alpha particles (Figure 7). We can see that the linear regression coefficient,  $R^2$ , is lower than for the response of the 4H-SiC detector to alpha particles. This is attributed to a difference in the amount of energy deposition in the active 4H-SiC detector area for alpha and gamma radiation. Due to the thickness of epitaxial layer and gamma energy deposition, we have not observed good correlation of 4H-SiC detector response with the active 4H-SiC detector area. A possible solution could be a fabrication of 4H-SiC detector with thicker epitaxial layer, as already implemented with high purity germanium detectors [3].

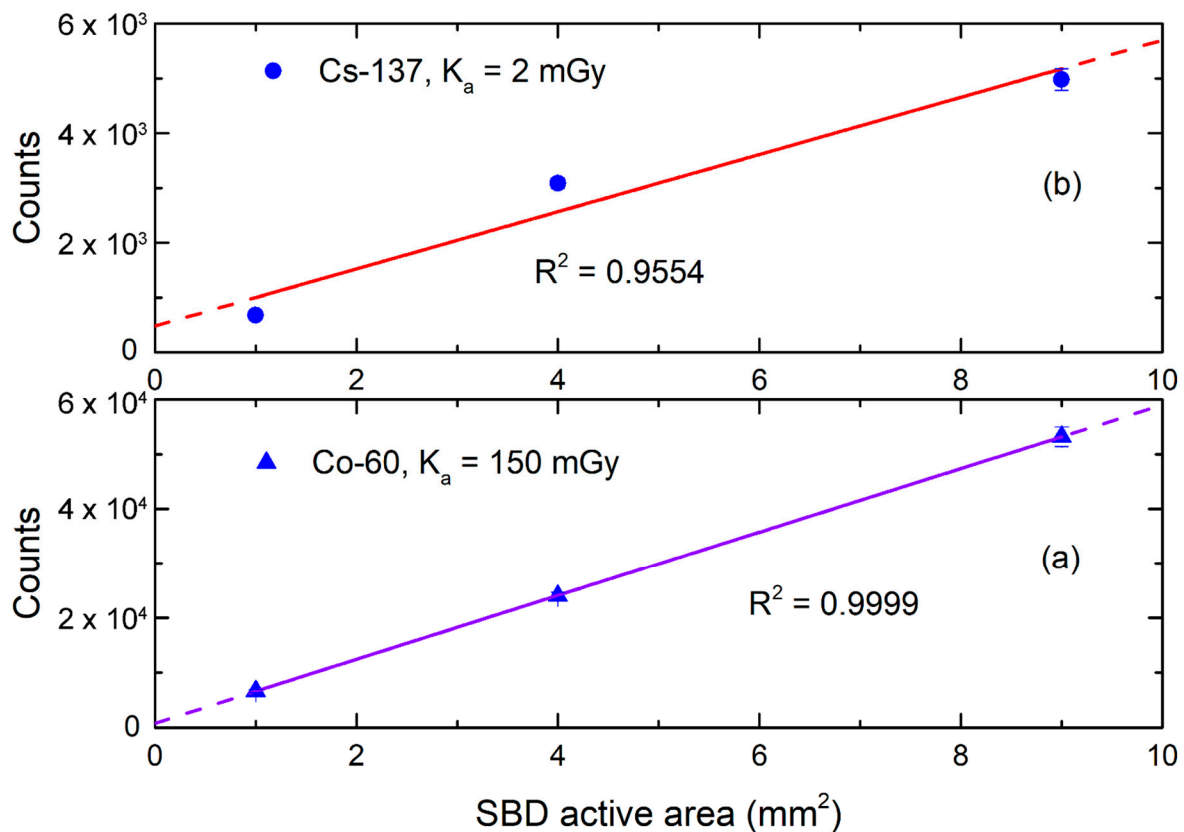


**Figure 10.** Response of three different 4H-SiC detector sizes ( $1 \times 1 \text{ mm}^2$ ,  $2 \times 2 \text{ mm}^2$  and  $3 \times 3 \text{ mm}^2$  active surface area) to gamma sources of Cs-137 (a) and Co-60 (b). Solid line in showing linear fit for three 4H-SiC detectors (active area of  $1 \times 1 \text{ mm}^2$ ,  $2 \times 2 \text{ mm}^2$  and  $3 \times 3 \text{ mm}^2$ ).

Results shown in Figures 8–10 lead to a conclusion that the signal in the low energy end of the pulse height spectra cannot be attributed to the electronic noise or interference as the counting efficiency is dependent on delivered air kerma.

#### 4. Discussion

Results of this study, combined with results of our tests published earlier, clearly demonstrate that the developed 4H-SiC detector based on the SBD configuration is capable not only of detecting charged particles and neutrons (directly or indirectly via neutron converters), but to detect gamma radiation in a counting mode as well. Electric characteristics of the SBDs did not change over consecutive exposure to different radiation fields, which demonstrates the radiation hardness of used 4H-SiC material. Free carrier concentration depth profiles did not change after the radiation testing. The  $Z_{1/2}$  deep level corresponding to carbon vacancy is the only observed defect in pristine and irradiated SiC material. Radiation tests with alpha and gamma sources have not introduced any changes in DLTS spectra.

The 4H-SiC detector shows a linear energy response for the alpha particle energies below 6.7 MeV, the threshold energy that corresponds to the range of alpha particles approximately equal to the whole thickness of the SiC epitaxial layer. We did not observe substantial increase of electronic noise with increasing active surface area of the 4H-SiC detector and the response is linear for all three different 4H-SiC detector active areas, which means that there is no decrease in sensitivity of the 4H-SiC detector with an increase in its active area. The best energy resolution of our detector system was 3%, for the Am-241 energy of 5486 keV and 3.3% for Gd-148 energy of 3183 keV.

Study of the 4H-SiC detector response in gamma radiation field of Co-60 and Cs-137 sources showed a linear response to air kerma and to different air kerma rates as well, up to

4.49 Gy/h. We have shown that the detector response is not in saturation for the dose rates lower than 15.3 mGy/min and that its measuring range for gamma radiation with energies of 662 keV, 1.17 MeV, and 1.33 MeV is from 0.5 mGy/h–917 mGy/h. The gamma response over the active 4H-SiC detector area is good. The linear regression coefficient  $R^2$ , is lower than 0.999, which is attributed to low CCE of the 4H-SiC detectors to gamma radiation. The sensitivity of the detector with the largest active area is not in linear correlation with the other to 4H-SiC detector active area sizes, and it decreases with the active area.

In summary, the obtained detector resolution of 3% for the wide alpha energy range combined with the linear response to gamma yield up to rates of 4.49 Gy/h demonstrates the usability of this detector system for the detection of special nuclear materials through detection of thermal neutrons and gamma decays.

**Supplementary Materials:** The following are available online at <https://www.mdpi.com/2073-4352/11/1/10/s1>, Figure S1: Measured electrical characteristics of 4H-SiC detector with active surface area of  $2 \times 2 \text{ mm}^2$  before and after radiation testing at room temperature (a) I-V characteristics and (b) C-V characteristics. Figure S2: Measured electrical characteristics of 4H-SiC detector with active surface area of  $2 \times 2 \text{ mm}^2$  before and after radiation testing at room temperature (a) I-V characteristics and (b) C-V characteristics.

**Author Contributions:** Formal analysis, R.B., L.B. and T.B.; investigation, R.B., I.C., L.B., T.B. and Ž.P.; resources, T.M., T.O. and A.S.; writing—original draft preparation, R.B., I.C. and L.B.; writing—review and editing, R.B., I.C., T.B., L.B., Ž.P., A.S., T.O. and T.M.; supervision, I.C. All authors have read and agreed to the published version of the manuscript.

**Funding:** This research was funded by NATO SPS Program, project number G5674. This research was partially funded by the National Collaborative Research Infrastructure Strategy (NCRIS) funding provided by the Australian Government. The RBI project team would like to acknowledge financial support from the European Regional Development Fund for the “Center of Excellence for Advanced Materials and Sensing Devices” (Grant No. KK.01.1.1.01.0001), “European Union’s Horizon 2020 Research and Innovation Programme, grant number 669014”, “European Union through the European Regional Development Fund—The Competitiveness and Cohesion Operational Programme, grant number KK.01.1.06”.

**Data Availability Statement:** Data is contained within the article or supplementary materials.

**Acknowledgments:** We would like to acknowledge Hidekazu Tsuchida and Norihiro Hoshino Central Research Institute of Electric Power Industry for the supply of SiC substrates with epitaxially grown 4H-SiC single-crystal layers.

**Conflicts of Interest:** The authors declare no conflict of interest. The funders had no role in the design of the study; in the collection, analyses, or interpretation of the data; in the writing of the manuscript, or in the decision to publish the results.

## References

1. Liu, L.Y.; Wang, L.; Jin, P.; Liu, J.L.; Zhang, X.P.; Chen, L.; Zhang, J.F.; Ouyang, X.P.; Liu, A.; Huang, R.H.; et al. The fabrication and characterization of Ni/4H-SiC schottky diode radiation detectors with a sensitive area of up to  $4 \text{ cm}^2$ . *Sensors* **2017**, *17*, 2334. [[CrossRef](#)] [[PubMed](#)]
2. Hedayati, R.; Lanni, L.; Rodriguez, S.; Malm, B.G.; Rusu, A.; Zetterling, C.M. A monolithic,  $500 \text{ }^\circ\text{C}$  operational amplifier in 4H-SiC bipolar technology. *IEEE Electron Device Lett.* **2014**, *35*, 693–695. [[CrossRef](#)]
3. Knoll, G.F. *Radiation Detection and Measurement*, 4th ed.; Wiley: Hoboken, NJ, USA, 2010.
4. Nava, F.; Bertuccio, G.; Cavallini, A.; Vittone, E. Silicon carbide and its use as a radiation detector material. *Meas. Sci. Technol.* **2008**, *19*, 102001. [[CrossRef](#)]
5. Sellin, P.J.; Vaitkus, J. New materials for radiation hard semiconductor detectors. *Nucl. Instrum. Methods Phys. Res. Sect. A Accel. Spectrometers Detect. Assoc. Equip.* **2006**, *557*, 479–489. [[CrossRef](#)]
6. Tudisco, S.; La Via, F.; Agodi, C.; Altana, C.; Borghi, G.; Boscardin, M.; Bussolino, G.; Calcagno, L.; Camarda, M.; Cappuzzello, F.; et al. Sicilia—silicon carbide detectors for intense luminosity investigations and applications. *Sensors* **2018**, *18*, 2289. [[CrossRef](#)] [[PubMed](#)]
7. Morales-Chávez, J.; Herrera-Celis, J.; Saldana-Ahuactzi, Z.; Reyes-Betanzo, C.; Gómez-Montaño, F.J.; Orduña-Díaz, A. Silicon and hydrogenated amorphous silicon carbide as biofunctional platforms for immunosensors. *Surf. Interfaces* **2020**, *20*, 100550. [[CrossRef](#)]

8. Naderi, N.; Moghaddam, M. Ultra-sensitive UV sensors based on porous silicon carbide thin films on silicon substrate. *Ceram. Int.* **2020**, *46*, 13821–13826. [[CrossRef](#)]
9. Verdon, C.; Szwedek, O.; Allemand, A.; Jacques, S.; Le Petitcorps, Y.; David, P. High temperature oxidation of two- and three-dimensional hafnium carbide and silicon carbide coatings. *J. Eur. Ceram. Soc.* **2014**, *34*, 879–887. [[CrossRef](#)]
10. Nava, F.; Vanni, P.; Bruzzi, M.; Lagomarsino, S.; Sciortino, S.; Wagner, G.; Lanzieri, C. Minimum ionizing and alpha particles detectors based on epitaxial semiconductor silicon carbide. *IEEE Trans. Nucl. Sci.* **2004**, *51*, 238–244. [[CrossRef](#)]
11. Ruddy, F.H.; Seidel, J.G.; Chen, H.; Dulloo, A.R.; Ryu, S.H. High-resolution alpha-particle spectrometry using 4H silicon carbide semiconductor detectors. *IEEE Trans. Nucl. Sci.* **2006**, *53*, 1713–1718. [[CrossRef](#)]
12. Radulović, V.; Yamazaki, Y.; Pastuović, Ž.; Sarbutt, A.; Ambrožič, K.; Bernat, R.; Ereš, Z.; Coutinho, J.; Ohshima, T.; Capan, I.; et al. Silicon carbide neutron detector testing at the JSI TRIGA reactor for enhanced border and port security. *Nucl. Instruments Methods Phys. Res. Sect. A Accel. Spectrometers Detect. Assoc. Equip.* **2020**, *972*, 164122. [[CrossRef](#)]
13. Hodgson, M.; Lohstroh, A.; Sellin, P.; Thomas, D. Characterization of silicon carbide and diamond detectors for neutron applications. *Meas. Sci. Technol.* **2017**, *28*, 105501. [[CrossRef](#)]
14. Pini, S.; Bruzzi, M.; Bucciolini, M.; Borchi, E.; Lagomarsino, S.; Menichelli, D.; Miglio, S.; Nava, F.; Sciortino, S. High-bandgap semiconductor dosimeters for radiotherapy applications. *Nucl. Instrum. Methods Phys. Res. Sect. A Accel. Spectrom. Detect. Assoc. Equip.* **2003**, *514*, 135–140. [[CrossRef](#)]
15. Moscatelli, F. Silicon carbide for UV, alpha, beta and X-ray detectors: Results and perspectives. *Nucl. Instrum. Methods Phys. Res. Sect. A Accel. Spectrom. Detect. Assoc. Equip.* **2007**, *583*, 157–161. [[CrossRef](#)]
16. Palestini, C. *Advanced Technologies for Security Applications*; Springer: Dordrecht, The Netherlands, 2019; ISBN 9789402420234.
17. Mandal, K.C.; Kleppinger, J.W.; Chaudhuri, S.K. Advances in high-resolution radiation detection using 4h-sic epitaxial layer devices. *Micromachines* **2020**, *11*, 254. [[CrossRef](#)]
18. Ruddy, F.H.; Dulloo, A.R.; Seidel, J.G.; Palmour, J.W.; Singh, R. The charged particle response of silicon carbide semiconductor radiation detectors. *Nucl. Instrum. Methods Phys. Res. Sect. A Accel. Spectrom. Detect. Assoc. Equip.* **2003**, *505*, 159–162. [[CrossRef](#)]
19. Ivanov, A.M.; Kalinina, E.V.; Kholuyanov, G.; Strokán, N.B.; Onushkin, G.; Konstantinov, A.O.; Hallén, A.; Kuznetsov, A.Y. High Energy Resolution Detectors Based on 4H-SiC. *Mater. Sci. Forum* **2005**, *483–485*, 1029–1032. [[CrossRef](#)]
20. Coutinho, J.; Torres, V.J.B.; Capan, I.; Brodar, T.; Ereš, Z.; Bernat, R.; Radulović, V. Silicon carbide diodes for neutron detection. *Nucl. Inst. Methods Phys. Res. A* **2020**, *986*, 164793. [[CrossRef](#)]
21. Flammang, R.W.; Seidel, J.G.; Ruddy, F.H. Fast neutron detection with silicon carbide semiconductor radiation detectors. *Nucl. Instrum. Methods Phys. Res. Sect. A Accel. Spectrom. Detect. Assoc. Equip.* **2007**, *579*, 177–179. [[CrossRef](#)]
22. Lioliou, G.; Chan, H.K.; Gohil, T.; Vassilevski, K.V.; Wright, N.G.; Horsfall, A.B.; Barnett, A.M. 4H-SiC Schottky diode arrays for X-ray detection. *Nucl. Instrum. Methods Phys. Res. Sect. A Accel. Spectrom. Detect. Assoc. Equip.* **2016**, *840*, 145–152. [[CrossRef](#)]
23. Ito, M.; Storasta, L.; Tsuchida, H. Development of 4H-SiC epitaxial growth technique achieving high growth rate and large-area uniformity. *Appl. Phys. Express* **2008**, *1*, 2–5. [[CrossRef](#)]
24. Lang, D.V. Deep-level transient spectroscopy: A new method to characterize traps in semiconductors. *J. Appl. Phys.* **1974**, *45*, 3023–3032. [[CrossRef](#)]
25. Peaker, A.R.; Markevich, V.P.; Coutinho, J. Junction spectroscopy techniques and deep-level defects in semiconductors. *J. Appl. Phys.* **2018**, *123*, 161559. [[CrossRef](#)]
26. Son, N.T.; Trinh, X.T.; Løvlie, L.S.; Svensson, B.G.; Kawahara, K.; Suda, J.; Kimoto, T.; Umeda, T.; Isoya, J.; Makino, T.; et al. Negative-U system of carbon vacancy in 4H-SiC. *Phys. Rev. Lett.* **2012**, *109*, 23–27. [[CrossRef](#)] [[PubMed](#)]
27. Capan, I.; Brodar, T.; Pastuović, Z.; Siegele, R.; Ohshima, T.; Sato, S.I.; Makino, T.; Snoj, L.; Radulović, V.; Coutinho, J.; et al. Double negatively charged carbon vacancy at the h- and k-sites in 4H-SiC: Combined Laplace-DLTS and DFT study. *J. Appl. Phys.* **2018**, *123*, 161597. [[CrossRef](#)]
28. Capan, I.; Brodar, T.; Coutinho, J.; Ohshima, T.; Markevich, V.P.; Peaker, A.R. Acceptor levels of the carbon vacancy in 4H-SiC: Combining Laplace deep level transient spectroscopy with density functional modeling. *J. Appl. Phys.* **2018**, *124*, 245701. [[CrossRef](#)]
29. Booker, I.D.; Hassan, J.U.; Lilja, L.; Beyer, F.C.; Karhu, R.; Bergman, J.P.; Danielsson, Ö.; Kordina, O.; Sveinbjörnsson, E.Ö.; Janzén, E. Carrier lifetime controlling defects Z1/2 and RB1 in standard and chlorinated chemistry grown 4H-SiC. *Cryst. Growth Des.* **2014**, *14*, 4104–4110. [[CrossRef](#)]
30. Delacroix, D.; Guerre, J.P.; Leblanc, P.; Hickman, C.; Penney, B.C. Radionuclide and Radiation Protection Data Handbook. *Med. Phys.* **2003**, *30*, 277. [[CrossRef](#)]
31. Jarrell, J.; Stika, M.; Chaiken, M.; Simpson, M.; Blue, T.E.; Cao, L.R. Determination of the thickness of an electrodeposited thorium film with SiC alpha detectors. *J. Radioanal. Nucl. Chem.* **2017**, *311*, 1127–1133. [[CrossRef](#)]
32. Ziegler, J.F.; Ziegler, M.D.; Biersack, J.P. SRIM-The stopping and range of ions in matter. *Nucl. Instrum. Methods Phys. Res. Sect. B Beam Interact. Mater. Atoms* **2010**, *268*, 1818–1823. [[CrossRef](#)]
33. Ziegler, J.F.; Biersack, J.P. The Stopping and Range of Ions in Matter. In *Treatise Heavy-Ion Science*; Springer: Boston, MA, USA, 1985; pp. 93–129.